Fire Technology manuscript No.
(will be inserted by the editor)

Engineering Approach for Designing a Thermal Test of Real-scale Steel Beam Exposed to Localized Fire

Chao Zhang · Lisa Choe · John Gross · Selvarajah Ramesh · Matthew Bundy

Received: date / Accepted: date

Abstract This paper reports the design and results of a thermal test on heating of a 6 m long steel W beam subjected to a localized fire conducted at the National Fire Research Laboratory (NFRL) of the National Institute of Standards and Technology (NIST). A engineering approach was proposed to determine the heat release rate of the test fire. By the approach, a recently developed simple fire model was first used to approximately calculate the heat release rate and then a sophisticated model was used to check/refine the calculation. The concept of adiabatic surface temperature was used in the sophisticated model to represent the thermal boundary conditions at exposed surfaces in fire. The proposed approach successfully predicted the critical value of heat release rate of 500 kW to reach a target temperature of 500 °C in the test

C. Zhang
National Institute of Standards and Technology, Fire Research Division, 100 Bureau Drive, Stop 8666, Gaithersburg, MD 20899-8666, USA
Tel.: +1 301 9756695
E-mail: chao.zhang@nist.gov

L. Choe
National Institute of Standards and Technology, Fire Research Division, 100 Bureau Drive, Stop 8666, Gaithersburg, MD 20899-8666, USA

J. Gross
National Institute of Standards and Technology, Fire Research Division, 100 Bureau Drive, Stop 8666, Gaithersburg, MD 20899-8666, USA

S. Ramesh
National Institute of Standards and Technology, Fire Research Division, 100 Bureau Drive, Stop 8666, Gaithersburg, MD 20899-8666, USA

M. Bundy
National Institute of Standards and Technology, Fire Research Division, 100 Bureau Drive, Stop 8666, Gaithersburg, MD 20899-8666, USA

specimen. A calibration test was also conducted to understand the difference between the predicted and measured steel temperatures in the investigated test, and found that the sophisticated model over-predict the adiabatic surface temperatures which would contribute to the over-prediction of the steel temperatures. The error of the predicted maximum steel temperature in the test specimen was within 10%. The study reported here is not necessarily a validation of the sophisticated model, rather the study provides a successful case study using current knowledge and tools to design realistic and controlled fire tests.

Keywords Localized fire · Controllable test Steel beam FDS-FEM approach · Simple fire model · Fire Dynamics Simulator (FDS) · Adiabatic surface temperature · Finite element simulation · Plate thermometer · Temperature calculation · Experimental design

1 Introduction

The standard fire resistance test method has dominated structural fire protection design practice and remained almost unchanged over the past 100 years [1]. The limitations of the standard fire resistance test method have been generally recognized and usually include [2]: (1) the standard temperature-time curve may not be representative of any fire scenarios; and (2) the tested isolated members in the furnace may not adequately represent the behavior of the components in an entire structure. As a result, fire protection design based on the standard fire test does not adequately assess or simulate the actual level of safety of a structure exposed to fire.

Fires in the open or in large enclosures are characterized as localized fires. Examples of localized fires include: vehicle fires in open car parks [3] and transportation infrastructures [4], and small shop fires in transport terminal halls [5]. Study on the behavior of steel structures under localized fire conditions has been lagging behind that of fully developed compartment fire conditions. This has been the result of the historical perception that localized fires are usually less hazardous than fully developed compartment fires. Recent studies [6–8] found that due to thermal gradient, the failure mode of bare steel members in a localized fire could be significantly different from the mode of the members in the standard enclosure fire test, and the failure temperature of bare steel members in a localized fire might be hundreds of degrees lower than that in the standard fire. Here, failure temperature of a steel member is taken as the maximum temperature in the member when structural failure (e.g., global buckling) happens. Therefore, using the standard fire for fire resistance design of structures in large enclosure might not always provide adequate safety. Testing the behavior of steel members in localized fires provides additional insight on the performance of steel members and may be necessary to more fully understand performance in large enclosures. To date, there are a number of test data on steel members subjected to localized fire, notably

Hasemi's [9,10]. However, there is lack of test data on real-scale steel members subjected to localized fire.

Before the construction of the National Fire Research Laboratory at NIST [11], there were very limited number of facilities in the world that allows scientists and engineers to conduct research on the response of real-scale structural systems to realistic fire and mechanical loading under controlled laboratory conditions. The NFRL addresses these research needs as well as other fire research topics such as advanced firefighting technologies, engineered fire safety, material flammability reduction and wildland-urban interface fire research. The unique facility will enable large-scale experiments using fires up to 20 MW and will contribute to the technical basis for performance-based design methodologies for structures exposed to fire. This paper presents the design and results of a thermal test of a 6 meter long steel W-section beam subjected to a localized fire conducted at the NFRL. Localized fire is selected as the test fire for its simplicity, controllability, reproducibility, and, at the same time, its capability to simulate the non-uniform heating condition in realistic fires.

2 Design objective and procedure

Designing a test fire is challenging because there is limited guidelines on how to conduct localized fires to examine performance of steel members. The available test data on structures in simulated compartment fires, e.g., Kirby [12] and Vassart et al. [13], are valuable for investigating the performance of structures in fire but provide little information for designing a laboratory test with controllable and measurable fire because previous structural fire tests seldom measured the most important fire parameter - heat release rate [14].

Fig. 1 shows the beam test setup used in this study. The beam specimen was a W16×26 section made of ASTM A992 steel with a length of 6.17 m that was simply supported on two 5.5 m long W12×106 reaction columns anchored to the strong floor (the supported length is 5.87 m). The 1.83 m×1.83 m diagonal bracing modules were installed next to columns to restrain in-plane movement (displacements) of those reaction columns. The test setup was located under the 20 MW exhaust hood. The distance between the lower flange of the beam specimen and the strong floor was 1.6 m.

A 1 m square natural gas burner with design capacity of 1 MW was located below the center of the beam specimen to apply fire load. The heat release rate and the distance from the burner surface to the beam specimen can be adjusted. In this test, no structural loads were applied and the distance from the burner surface to the lower flange of the beam specimen was about 1.2 m. The objective of the design is to determine a heat release rate time history curve so that the test specimen can reach a maximum temperature of 500 °C.

Fig. 2 shows the proposed design procedure for the investigated test. This procedure can be initiated by specifying fire source area, beam specimen height and target steel temperature which remain constant. We endeavor to solve for the heat release rate (HRR). For the investigated case, an initial heat release

rate of 100 kW and a heat release rate increment of 100 kW ($\triangle HRR$=100 kW) are considered. A simple model (described later in Section 3) is first used to calculate a critical heat release rate at which the effective black body temperature (defined later by Eq. 5) is not less than the target steel temperature (Criterion I). Then, the critical heat release rate is used to run a FDS simulation (discussed later in Section 4.3.1). The maximum adiabatic surface temperature (defined later in Section 4.2) of the beam specimen, predicted by FDS, should be not less than the target steel temperature (Criterion II). Otherwise, the critical heat release rate is modified and the FDS simulation is rerun to meet the criterion (II). Finally, a finite element simulation (described later in Section 4.3.2) is conducted to get the temperature distribution of the beam specimen. The maximum steel temperature of the beam specimen should not be less than the target steel temperature (Criterion III), otherwise the critical heat release rate is modified and the FDS - FEM simulation (Section 4) is rerun to meet the criterion (III).

3 Heat release rate by approximate calculation

The theoretical model described in Ref. [15] was used as a simple approach to calculate the thermal radiation to a horizontal surface above a fire source, as shown in Fig. 3. In this approach, the fire plume volume is represented by a cylinder. The diameter of the cylinder is taken as the equivalent diameter of the fire source and the height of the cylinder is taken as the height of the bottom of the specimen. Flame and smoke are assumed to be gray and have the same emission coefficients, $\rho\kappa$. The temperatures in the horizontal cross sections of the cylinder are assumed to be uniform and taken as the centerline temperature of the fire plume calculated according to Ref. [16]. According to the model, the thermal radiation received by the bottom of the specimen is

$$E(H) = \int_0^H E_z dz \tag{1}$$

with

$$E_z(dz) = (1-\alpha)F\varepsilon\sigma \times (T_g + 273)^4 \tag{2}$$

where

$$\alpha(H-z) = 1 - e^{-\varrho\kappa(H-z)} \tag{3}$$

and

$$\varepsilon(dz) = 1 - e^{-\varrho\kappa dz} \tag{4}$$

where $\alpha(H-z)$ is the absorptivity of the cylinder volume with height $H-z$; $\varepsilon(dz)$ is the emissivity of the cylinder volume with height dz; σ is the Stefan-Boltzmann constant, taken as 5.67×10^{-8} W/(m^{2}K^4); T_g is the centerline gas temperature; and F is the view factor between two parallel circular surfaces calculated by the equations in Fig. 3.

From Eq 1, an effective black body temperature of the exposed surface at the bottom of the specimen can be defined as:

$$T_{beff}(H) = \sqrt[4]{\frac{E(H)}{\sigma}} - 273 \quad (5)$$

The temperature of the exposed surface cannot exceed the calculated effective black body temperature [1].

Assuming effective emission coefficient as 6.45 m^{-1} (as for methane [17]) and radiative loss fraction as 0.2, Table 1 shows the calculated effective black body temperature at the bottom of the specimen $T_{beff}(1.2)$ (H =1.2 m) for various HRR values. The flame length L_f and centerline gas temperatures at the bottom $T_g(1.2)$, predicted by the plume theory [16], are also presented. Fig. 4 shows the fire plume centerline temperatures for the 1 m square burner with various heat release rates. For HRR greater than or equal to 400 kW, L_f is greater than 1.2 m (the flame touches the specimen bottom) and $T_{beff}(1.2)$ is greater than 500 °C. Therefore, in order to achieve a maximum steel temperature of 500 °C the HRR should be not less than 400 kW (heat release rate increment in the test is taken as 100 kW).

Table 1 also shows that the effective black body temperature is first higher (for $HRR < 700$ kW) and then lower than the gas temperature (for $HRR >= 700$ kW). This can be explained by the fact that the gas temperature drops off faster than the radiation temperature above the flames.

4 Heat release rate by sophisticated simulation

4.1 The FDS-FEM approach

The simulation methodology described in Ref. [18] and similarly in [19] was used in this study. Fire Dynamics Simulator (FDS, version 6.1.1), a large-eddy simulation (LES) code developed by NIST [20], was utilized to predict the fire environment in the test. The thermal boundary conditions, at the exposed surfaces of the steel members, predicted by FDS were mapped into the thermal model in ANSYS, a commercial FEM (Finite Element Method) code [2] [21], to conduct heat transfer analysis to predict the temperature of the steel members. The following section describes the method for applying thermal boundary conditions in ANSYS using adiabatic surface temperatures predicted by FDS [3]

[1] Here, convection is not considered. For conditions where convection is dominant, the temperature of a exposed surface can be higher than the effective black body temperature calculated by Eq. 5

[2] Certain commercial entities, equipment, or materials may be identified in this document in order to describe an experimental procedure or concept adequately. Such identification is not intended to imply recommendation or endorsement by the National Institute of Standards and Technology, nor is it intended to imply that the entities, materials, or equipment are necessarily the best available for the purpose.

[3] Section 4.2 was taken from Ref. [18] with minor edition and is repeated here for its importance in understanding the FDS-FEM approach.

4.2 Adiabatic surface temperature

Consider an ideal adiabatic surface exposed to a heating condition, the net heat flux to the surface is by definition zero, thus

$$\varepsilon_{AS}(\dot{q}''_{in} - \sigma T_{AS}^4) + h_{c,AS}(T_g - T_{AS}) = 0 \tag{6}$$

where $\dot{q}''_{in}$ is the incident radiative flux; ε_{AS} is the emissivity of the adiabatic surface; T_{AS} is the temperature of the adiabatic surface; and $h_{c,AS}$ is the film coefficient between the adiabatic surface and the surrounding gas.

From Eq. 6, the incident radiative flux to a surface can be calculated from the adiabatic surface temperature,

$$\dot{q}''_{in} = \frac{h_{c,AS}(T_{AS} - T_g)}{\varepsilon_{AS}} + \sigma T_{AS}^4 \tag{7}$$

Consider a real surface exposed to the same heating condition, the net heat flux to the surface can be calculated by

$$\dot{q}'' = \varepsilon_s \dot{q}''_{in} - \dot{q}''_{emi} + h_c(T_g - T_s) \tag{8}$$

where T_s is the temperature of the real surface; and $\dot{q}''_{emi} = \varepsilon_s \sigma T_s^4$ is the emission of the real surface. If the emissivity of the adiabatic surface is taken as the emissivity of the real surface ($\varepsilon_{AS} = \varepsilon_s$), and the film coefficient between the adiabatic surface and the surrounding gas is equal to the film coefficient between the real surface and the surrounding gas ($h_{c,AS} = h_c$), Eq. 8 can be written as

$$\dot{q}'' = \varepsilon_s \sigma (T_{AS}^4 - T_s^4) + h_c(T_{AS} - T_s) \tag{9}$$

Eq. 9 shows that the net heat flux to a surface can be approximated using a single parameter, T_{AS}. FDS includes an output quantity of adiabatic surface temperature calculated by Eq. 9 according to the concept proposed by Wickstrom [22]. In the test, the adiabatic surface temperatures of interest can be measured using a plate thermometer [23].

4.3 Numerical models

4.3.1 The FDS model

Fig. 5 shows the FDS model geometry and computational mesh for the thermal test configuration. The beam sections (bottom flange, web and top flange) were modeled by obstructions with zero thickness. Dimensions of the computational domain are 7.2 m (X) × 1.6 m (Y) × 3.6 m (Z). The grid size used is an important numerical parameter in computational fluid dynamics because of its impact on numerical accuracy. The necessary spatial resolution for a proper

LES simulation of a free burning fire is customarily defined in terms of the characteristic diameter of a plume, D^*, which is defined as [20]

$$D^* = (\frac{\dot{Q}}{\rho_\infty c_p T_\infty \sqrt{g}})^{2/5} \tag{10}$$

where $\dot{Q}$ is the heat release rate; ρ_∞ is the ambient density; c_p is the specific heat of air at constant pressure; T_∞ is the ambient temperature; and g is the acceleration of gravity. The spatial resolution, R^*, of a numerical grid is defined as,

$$R^* = \frac{dx}{D^*} \tag{11}$$

where dx is characteristic length of a cell for a given grid. For the FDS model, the grids in the Y and Z directions were uniform (4 cm), while that in the X direction was stretched to yield the grid size in the flame region of 4 cm. Therefore, the resolution at the flame region was about 1/13 for HRR of 200 kW and about 1/21 for 700 kW. The computational domain consisted of 432,000 control volumes.

4.3.2 The FEM model

Fig. 6 shows the FEM model of the beam specimen for heat transfer analyses. The FEM model was meshed by SHELL131 element in ANSYS. As shown in 6a, SHELL131 is a 3D layered shell element having in-plane and through-thickness thermal conduction capability, and is applicable to a 3D, steady-state or transient thermal analysis. The divisions of the test specimen were 8 for flanges, 12 for web and 210 along beam length. Convection and thermal radiation were applied to the exposed surfaces, which were calculated using the adiabatic surface temperatures and film coefficients from FDS simulation. In the FEM model, temperature-dependent thermal properties for structural steel specified in the Eurocode [24] were used. The same emissivity of steel was used in the FDS and FEM simulations.

4.4 Numerical results

4.4.1 FDS predictions

Fig. 7 shows the simulated flame geometry for various HRRs. Note that the flame shape changes with time because of the turbulent combustion processes. For HRR greater than or equal to 400 kW, the flame touches the bottom of the beam specimen, which is consistent with the approximate calculation prediction. Fig. 8 shows the spatial distributions of adiabatic surface temperature with increasing HRR. Fig. 9 shows the time averaged adiabatic surface temperatures along the beam length for each maintained HRR from 200 kW to 700 kW. Note that the unsmoothness of the curves or "steps" in Fig. 9

are caused by the fact that the measured value of a device point located in a computational cell in FDS is taken as the value of the nearby grid point and ,therefore, two device points located at two sides of a cell surface may output a same temperature. For the bottom surface of the beam specimen (points 1 or 2 in Fig. 9), the adiabatic surface temperature increases with HRR until a peak value, which is similar to the trend shown in Table 1 where T_{beff} becomes constant as HRR becomes greater than or equal to 700 kW. While flame length increases with HRR, the portion of the flame that contributes radiation to the bottom surface, which determines AST or T_{beff}, becomes constant once HRR reaches a critical value (e.g., 800 kW in Table 1). Because of the shield effect, the adiabatic surface temperatures for the bottom surface (point 1) are higher than those for the other surfaces.

4.4.2 FEM predictions

The FEM predicted maximum steel temperatures are 381 °C, 500 °C, 587 °C, and 646 °C for each maintained HRR of 300 kW, 400 kW, 500 kW, and 600 kW at steady state. Fig. 10 shows the temperature distribution in the test specimen for a maintained HRR of 400 kW at steady state. By FEM calculation, the steel temperature does not reach 500 °C if the HRR is less than 400 kW. This is consistent with the approximate calculation result. When the HRR is increased with an increment of 100 kW every 5 min, the target steel temperature of 500 °C is predicted at 1371 s after ignition with a corresponding HRR of 500 kW. Note that the target temperature here means the maximum section temperature at the moment but not the final/ultimate temperature that would be reached if the exposure would continue for a longer duration.

5 Fire test results and discussion

Fig. 11 shows the measured heat release rate curve for the thermal test. The stepped heat release rate curve with increment of 100 kW per 5 min is also presented for reference. In the test, the gas flow of the burner was controlled manually that the measured heat release rate curve didn't adequately fellow the designed stepped curve. The heating test stopped at about 1685 s after ignition when the temperatures measured by thermocouples reached about 500 °C. At that time, the measured heat release rate was about 500 kW, which was consistent with the numerical prediction.

In the test, the flame shape was found to be asymmetric (Fig. 12), which is caused by the opening of mechanical vents that caused asymmetric air flow in the test zone. As a results, the steel temperature measured by the thermocouples located at symmetrical positions (e.g. TC_30 and TC_29 shown in Fig. 13) had considerable difference. In Fig. 13, the red hash marks on the beam cross-section symbolize thermocouples, and the thermocouples (e.g. 24, 17, 10) are at different locations along the beam length. Based on the observation from this test, in the subsequent tests conducted at the NFRL, the mechanical vents

were adjusted and tape lines were installed at the four corner of the test zone to check the uniformity of the air flow.

In the real test, two rectangular burners with area of 0.5 m^2 each were assembled to generate a burning area of 1 m^2. The gap between those two burners was about 5 cm $\pm$ 1 cm. To better understand the heating mechanism of steel beams exposed to localized fire, post-test simulations were conducted using the measured heat release rate curve. Two burning areas according to the real test setup were used. The grid size in the flame region was 2 cm.

Fig. 14 compares the measured and predicted steel temperatures for the thermal test. For the center section (section 6), the numerical approach predicted maximum steel temperature is about 50 °C (10%) higher than the measured value (TC_30). For section 5 (Fig. 13), the predicted maximum steel temperature is about 41 °C (9%) lower than the measured value (TC_23). Note that the differences between the measured and predicted steel temperatures during the heating process could be much bigger than the differences at the end of heating.

A calibration test using a maintained heat release rate of 400 kW was conducted in order to understand the difference between the predicted and measured steel temperatures in the thermal test. Fig. 15 shows the layout of plate thermometers (PTs) in the calibration test. Fig. 16 compares the measured and predicted temperatures for the plate thermometers. For PT_1, FDS gives good predictions; and for other PTs, FDS gives over-predictions at high temperatures. The large difference between the measured and predicted temperatures for PT_2 might also be caused by non-symmetrical vent condition during the test [4], as shown in Fig. 12. The difference between measured and predicted PT temperatures (or adiabatic surface temperatures) is consistent with the difference between the measured and predicted steel temperatures. The over-prediction of the adiabatic surface temperatures (PT temperatures) contributes to the over-prediction of the maximum steel temperatures.

In this paper, thermocouple error and digitization error were derived from instrument specifications, while the thermocouple installation error was estimated from past experience. The test repeatability was derived from the temperature measurements from two identical tests. The components of combined uncertainty for temperature included manufacturers specifications on thermocouple error of 0.4%, digitization error of 3.2 °C, positioning error of 10 °C, and test repeatability of 12.6 °C. The measured temperatures have a total expanded uncertainty of 33 °C which was calculated from a combined uncertainty of 16.6 °C and a coverage factor of 2 with a level of confidence of approximately 95 percent. The uncertainty in the HRR measurements with a natural gas burner is presented in Bryant et al. [25] and not presented here for brevity.

[4] The boundary conditions for the computational domain in the FDS model was assumed to be symmetrical but in the test the opening of mechanical vents caused asymmetric air flow in the test zone.

6 Conclusions

The structural fire safety design practice is moving from following the rules specified in prescriptive codes toward performance-based fire safety design which requires a deep understanding on the performance of structures in realistic fires. For the structural fire tests reported in literature, most of them were conducted in an enclosed furnace, some were conducted in real compartment (e.g. the Cardington full-scale fire tests) and few of them were conducted in an open condition (e.g. a localized fire condition). Besides, all those tests seldom measured the heat release rate of the fire. There is little guideline on how to test the performance of structures in realistic fires. A primary and also challenging problem in the realistic fire testing (on structures) is how to select and design the test fire. This paper proposed an engineering approach to design a test fire for evaluating the performance of structures in large enclosure. Localized fire is selected as the test fire and the approach is developed to determine the critical heat release rate of the localized fire to achieve a target temperature in the test specimen. The proposed approach was successfully applied to design a thermal test on a real-scale steel beam exposed to a localized fire recently conducted at the NFRL. The application of the proposed approach is not limited to the studied case but also includes any other cases using localized fire as the test fire.

Acknowledgements Thanks to Drs. Craig Weinschenk, Randall McDermott, and Kevin McGrattan of NIST for their support in developing and improving the numerical models. Thanks to Dr. Christopher Smith of NIST for his helpful comments on explaining the experimental results. Thanks to Mr. Nelson Bryner of NIST for his comments on measurement uncertainties in the test. Valuable suggestions and review comments from Drs. Anthony Hamins and Dat Duthinh of NIST are acknowledged.

References

1. S.H. Ingberg, H.K. Griffin, W.C. Robinson, and R.E. Wilson. Fire tests of building columns. Technologic papers no. 184, Bureau of Standards, 1921.
2. L. Bisby, J. Gales, and C. Maluk. A contemporary review of large-scale non-standard structural fire testing. *Fire Science Reviews*, 2:1–27, 2013.
3. B. Zhao and J. Kruppa. Structural behaviour of an open car park under real fire scenarios. *Fire and Materials*, 28:269–280, 2004.
4. H. Mostafaei, M. Sultan, and A. Kashef. Resilience assessment of critical infrastructure against extreme fires. In *Proceedings of the 8th International Conference on Structures in Fire*, pages 1153–1160, 2014.
5. W.K. Chow. Assessment of fire hazard in small news agents in transport terminal halls. *Journal of Architectural Engineering*, 11:35–38, 2005.
6. C. Zhang, G.Q. Li, and A. Usmani. Simulating the behavior of restrained steel beams to flame impinged localized fires. *Journal of Constructional Steel Research*, 83:156–65, 2013.
7. C. Zhang, J.L. Gross, and T. McAllister. Lateral torsional buckling of steel w-beams to localized fires. *Journal of Constructional Steel Research*, 88:330–8, 2013.
8. C. Zhang, J.L. Gross, T.P. McAllister, and G.Q. Li. Behavior of unrestrained and restrained bare steel columns subjected to localized fire. *Journal of Structural Engineering-ASCE*, 141, 2015.

Table 1 Simple model calculation

HRR	200 kW	300 kW	400 kW	500 kW	600 kW	700 kW	800 kW	900 kW
L_f	0.81 m	1.16 m	1.44 m	1.68 m	1.89 m	2.09 m	2.27 m	2.43 m
$T_g(1.2)$	318 °C	457 °C	602 °C	757 °C	923 °C	1101 °C	1210 °C	1210 °C
$T_{beff}(1.2)$	336 °C	498 °C	665 °C	831 °C	983 °C	1099 °C	1126 °C	1126 °C

9. Y. Hasemi, Y. Yokobayashi, T. Wakamatsu, and A. Ptchelintsev. Modeling of heating mechanism and thermal response of structural components exposed to localized fires: A new application of diffusion flame modeling to fire safety engineering. NIST internal report 6030, National Institute of Standards and Technology (NIST), Gaithersburg, Maryland, 2010.
10. D. Kamikawa, Y. Hasemi, K. Yamada, and M. Nakamura. Mechanical response of a steel column exposed to a localized fire. In *Proceedings of the Fourth International Workshop on Stuctures in Fire*, pages 225–34, Aveiro, Portugal, 2006.
11. M. Bundy, A. Hamins, J. Gross, W. Grosshandler, and L. Choe. Structural fire experimental capabilities at the nist national fire research laboratory. *Fire Technology*, 2016.
12. B.R. Kirby. Large scale fire tests: the british steel european collaborative research programme on the bre 8-storey frame. *Fire Safety Science*, 5:1129–1140, 1997.
13. O. Vassart, C.G. Bailey, A. Nadjai, W.I. Simms, B. Zhao, T.Gernay, and J.M. Franssen. Large-scale fire test of unprotected cellular beam acting in membrane action. *Structures and Buildings*, 165:327–334, 2012.
14. V. Babrauskas and R.D. Peacock. Heat release rate: The single most important variable in fire hazard. *Fire Safety Journal*, 18:255–272, 1992.
15. C. Zhang and A. Usmani. Heat transfer principles in thermal calculation of structures in fire. *Fire Safety Journal*, 78:85–95, 2015.
16. C. Zhang and G.Q. Li. Fire dynamic simulation on thermal actions in localized fires in large enclosure. *Advanced Steel Construction*, 8:124–36, 2012.
17. C.L. Tien, K.Y. Lee, and A.J. Stretton. *Radiation heat transfer. SFPE handbook of fire protection engineering, 3rd edition, Section 1-4*. National Fire Protection Association, 2003.
18. C. Zhang, J. Silva, C. Weinschenk, D. Kamikawa, and Y. Hasemi. Simulation methodology for coupled fire-structure analysis: modeling localized fire tests on a steel column. *Fire Technology*, 52:239–262, 2015.
19. D. Duthinh, K.B. McGrattan, and A. Khaskia. Recent advances in fire-structure analysis. *Fire Safety Journal*, 43:161–7, 2008.
20. K. McGrattan, S. Hostikka, R. McDermott, J. Floyd, C. Weinschenk, and K. Overholt. *Fire Dynamics Simulator, User's Guide*. National Institute of Standards and Technology, Gaithersburg, Maryland, USA, and VTT Technical Research Centre of Finland, Espoo, Finland, sixth edition, September 2013.
21. ANSYS. *ANSYS User Mannual, Version 14.0*. ANSYS Inc., 2012.
22. U. Wickstrom, D. Duthinh, and K.B. McGrattan. Adiabatic surface temperature for calculating heat transfer to fire exposed structures. In *Proceedings of the 11the International Interflam Conference*, pages 943–53, London, England, 2007.
23. U. Wickstrom. The plate thermometer - a simple instrument for reaching harmonized fire resistance tests. *Fire Technology*, 30:195–208, 1994.
24. BSI. *Eurocode 3: Design of steel structures - Part 1-2: General rules - Structural fire design*. British Standard, 2005.
25. R. Bryant, M. Bundy, and R. Zong. Evaluating measurements of carbon dioxide emissions using a precision source - a natural gas burner. *Journal of the Air & Waste Management Association*, 65:863–870, 2015.

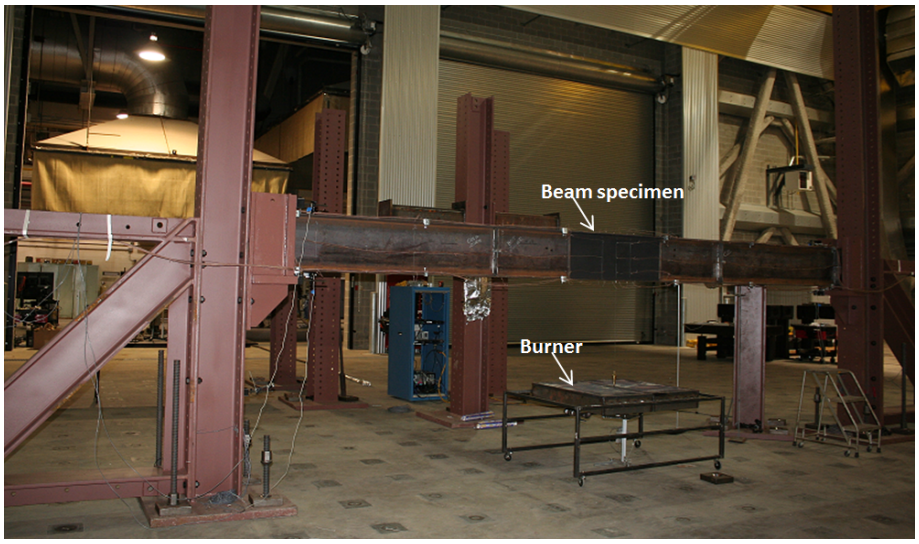

Fig. 1 Experimental steup.

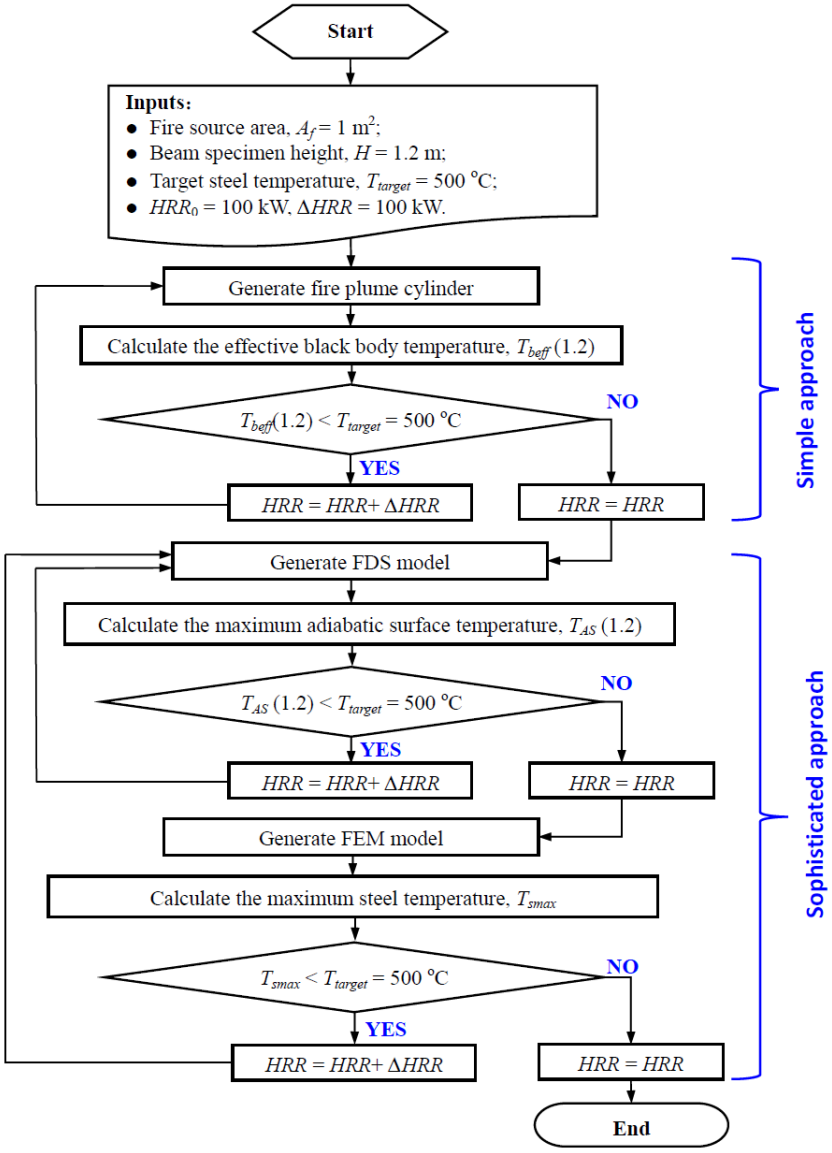

Fig. 2 Procedure for determining a heat release rate to reach a target temperature.

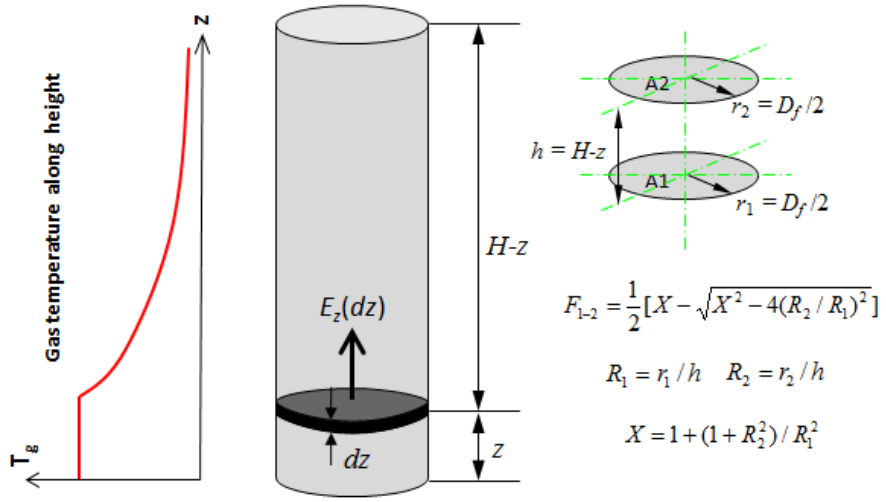

Fig. 3 A theoretical model to calculate the radiation to an horizontal components in a localized fire [15].

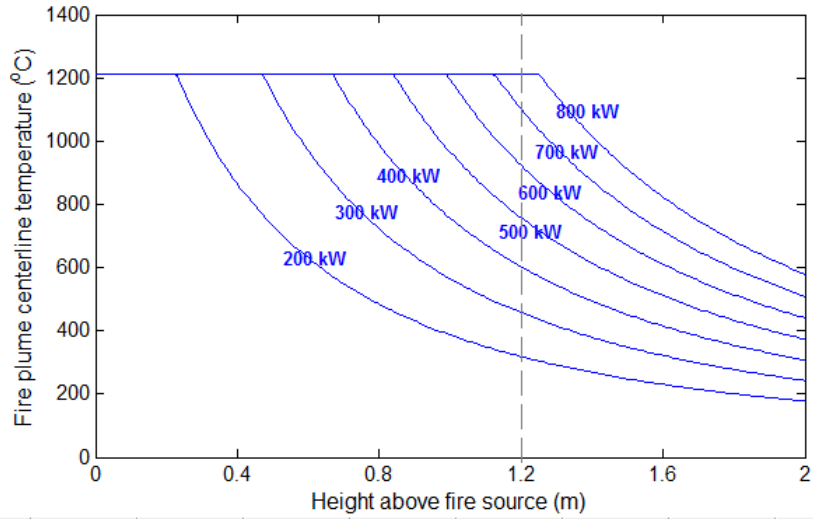

Fig. 4 Fire plume centerline temperatures for the 1 m square burner with various HRR, calculated according to [16].

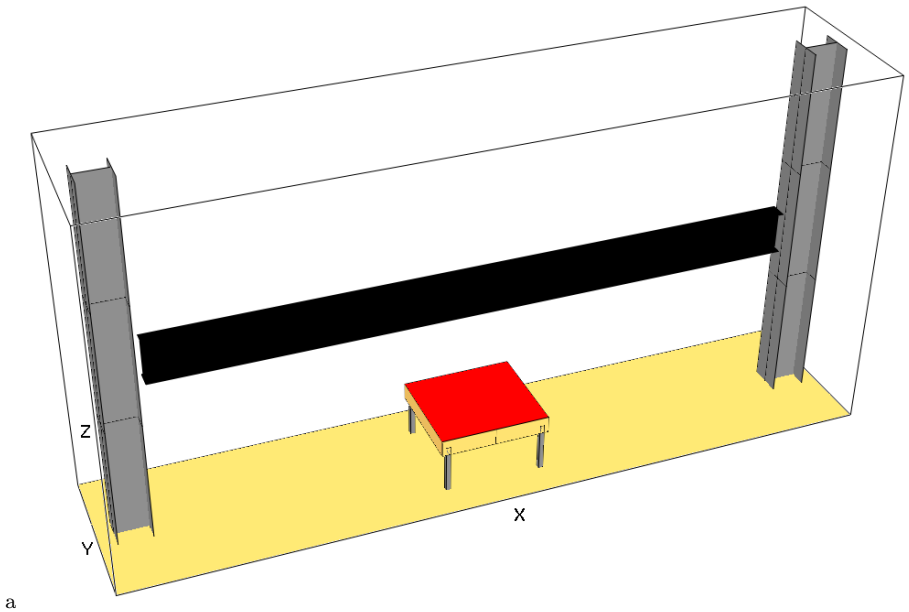

a

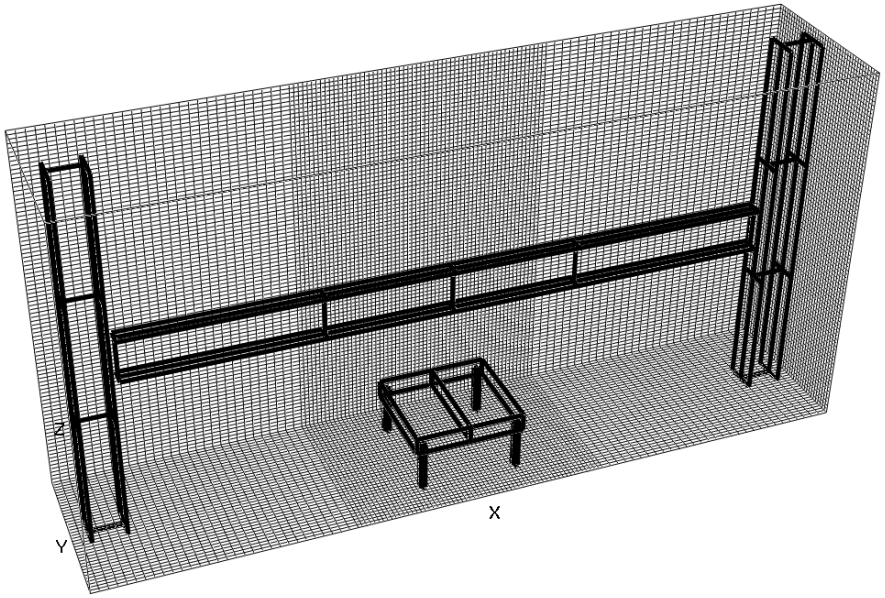

b

Fig. 5 FDS model for pre-test simulation of the NFRL commissioning thermal tests.

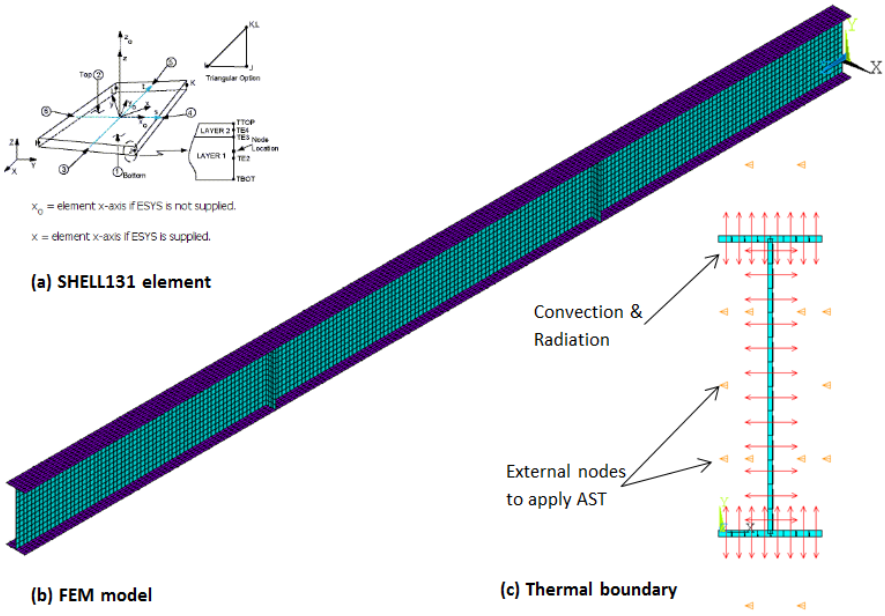

Fig. 6 FE model for the NFRL commissioning thermal tests.

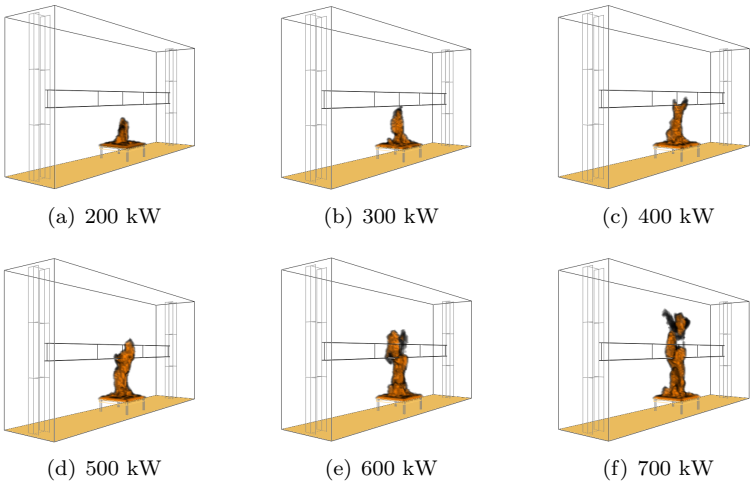

(a) 200 kW (b) 300 kW (c) 400 kW

(d) 500 kW (e) 600 kW (f) 700 kW

Fig. 7 FDS simulated flame behavior for various constant HRRs.

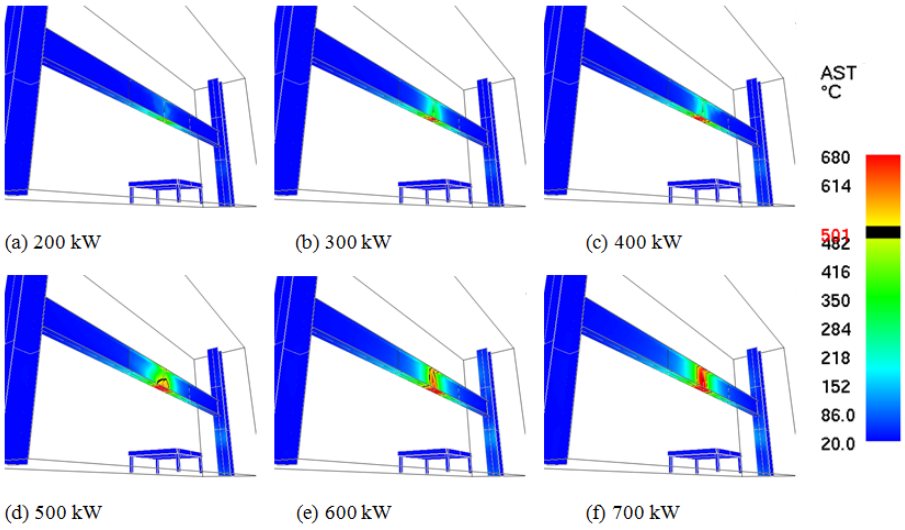

(a) 200 kW (b) 300 kW (c) 400 kW

(d) 500 kW (e) 600 kW (f) 700 kW

Fig. 8 FDS predicted adiabatic surface temperature for various constant HRRs.

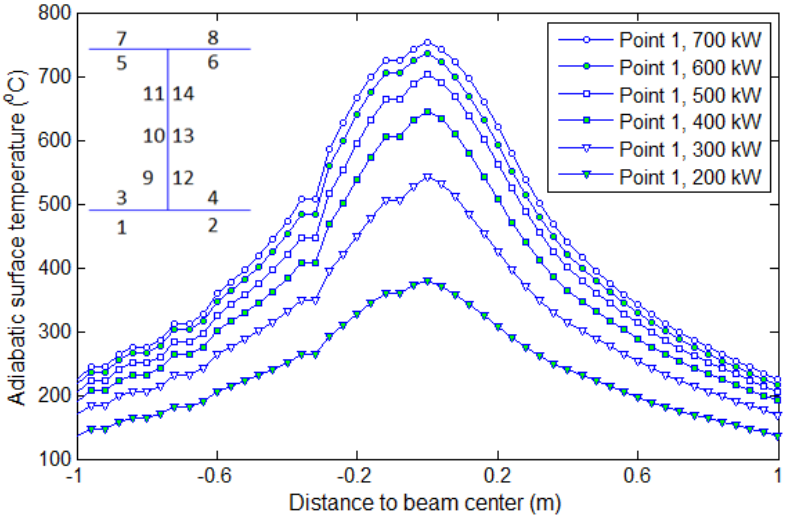

(a)

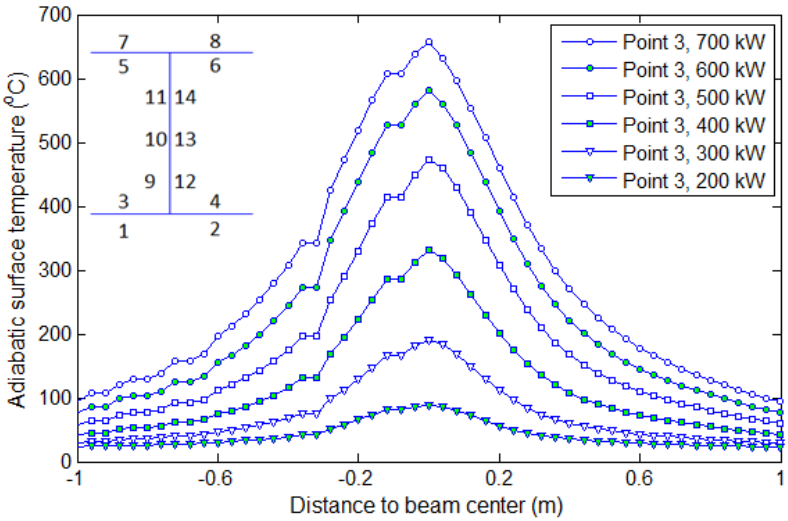

(b)

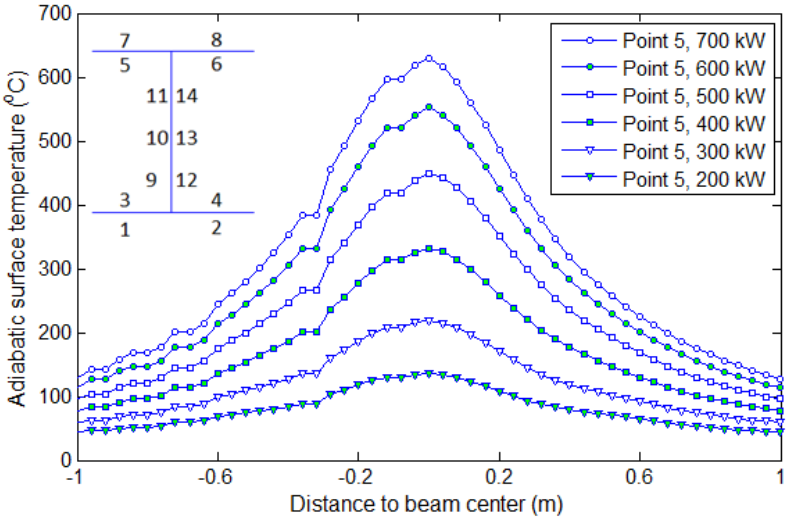

(c)

Fig. 9 FDS predicted adiabatic surface temperature along beam length.

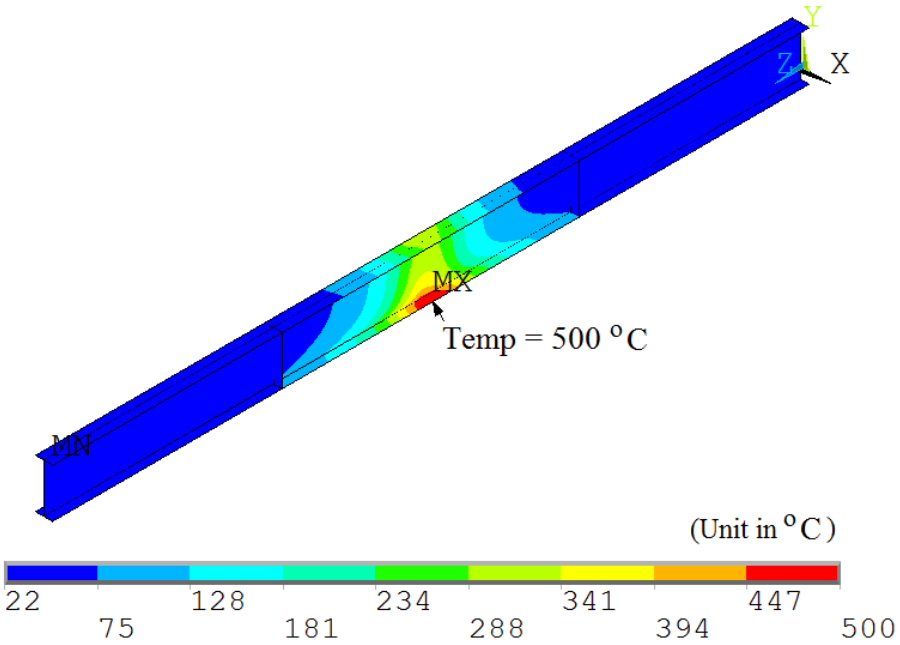

Fig. 10 FE predicted maximum steel temperature distribution in the test specimen for constant heat release rate of 400 kW.

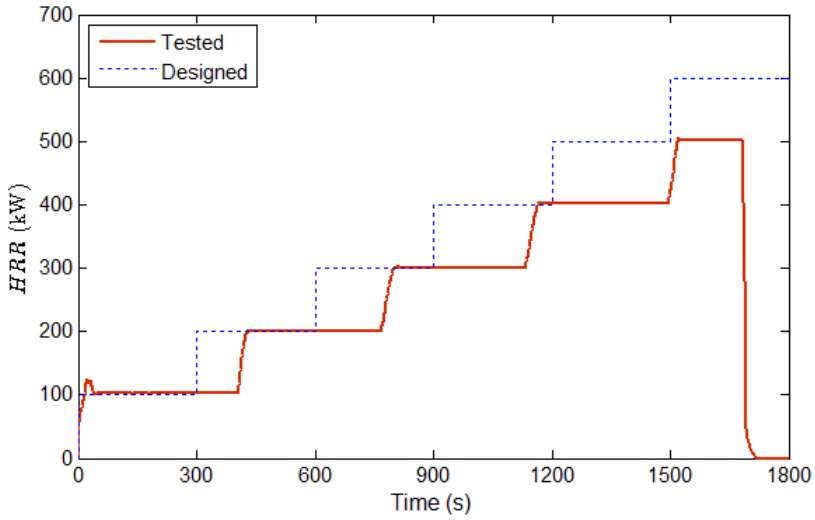

Fig. 11 Measured heat release rate for NFRL commissioning thermal test 1.

Fig. 12 A photograph of the flame during the NFRL commissioning thermal test 1.

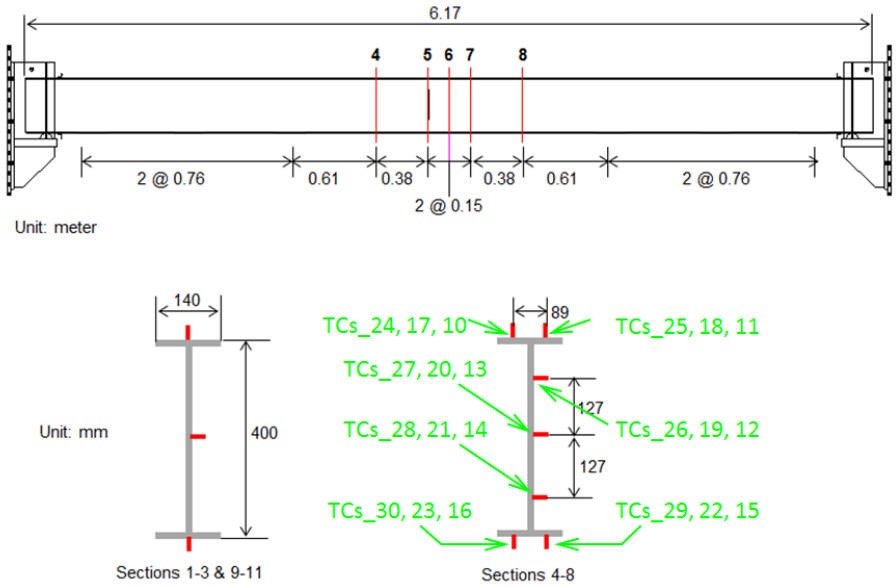

Fig. 13 Layout of the thermocouples for the NFRL commissioning thermal tests.

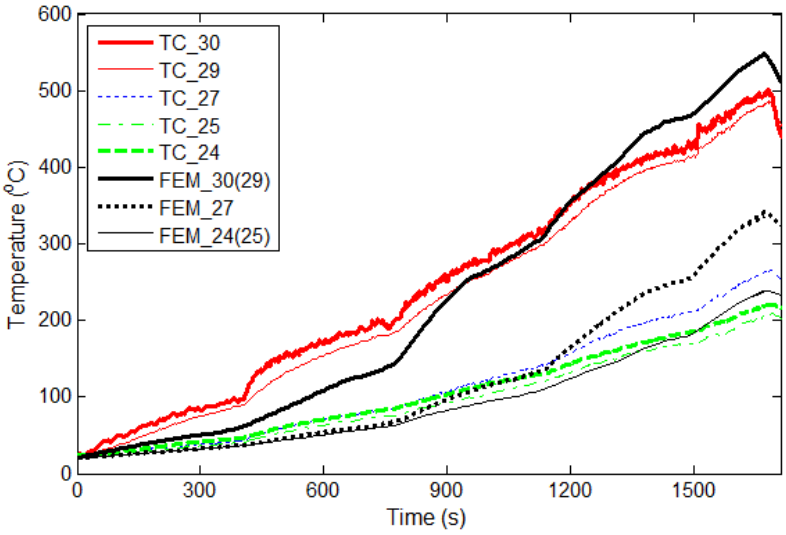

(a) section 6

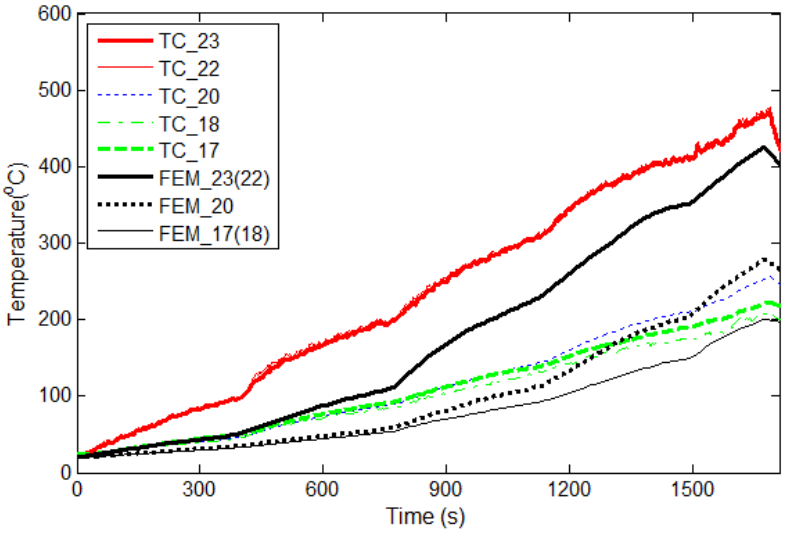

(b) section 5

Fig. 14 Comparison between the measured and predicted steel temperatures for NFRL commissioning thermal test 1.

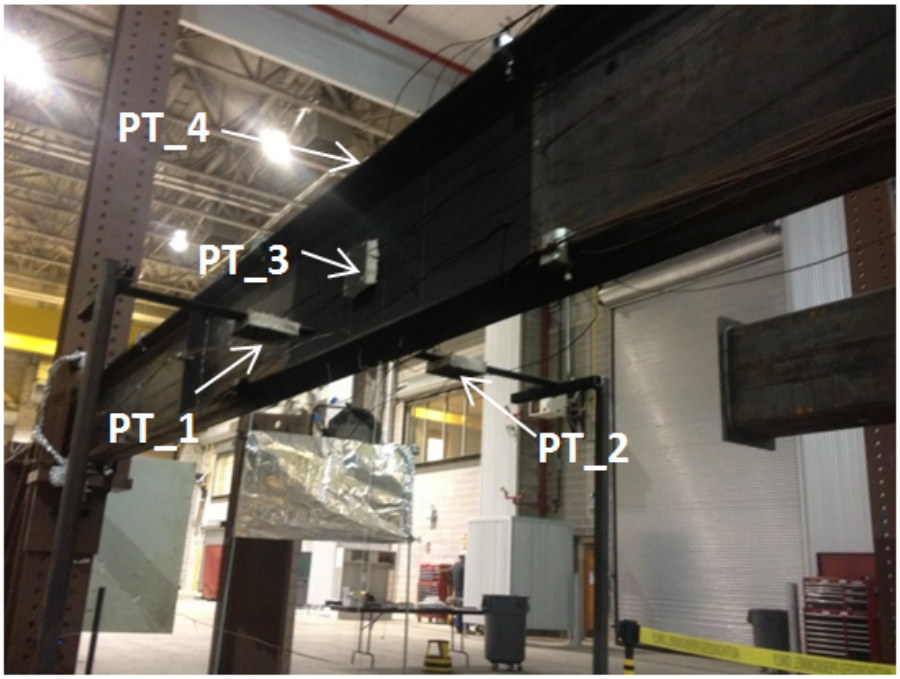

(a)

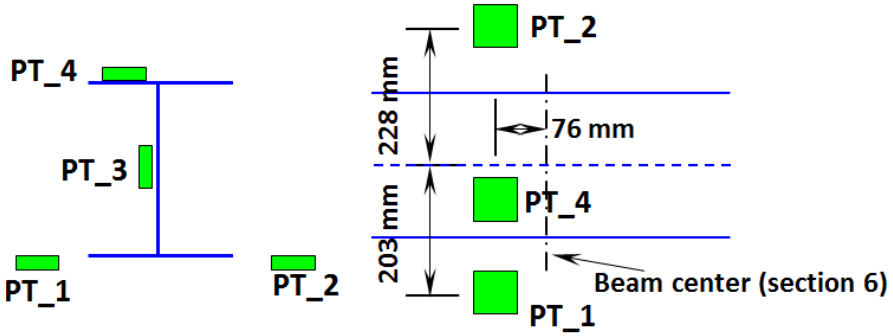

(b)

Fig. 15 Location of plate thermometers (PTs) in NFRL commissioning thermal test 3.

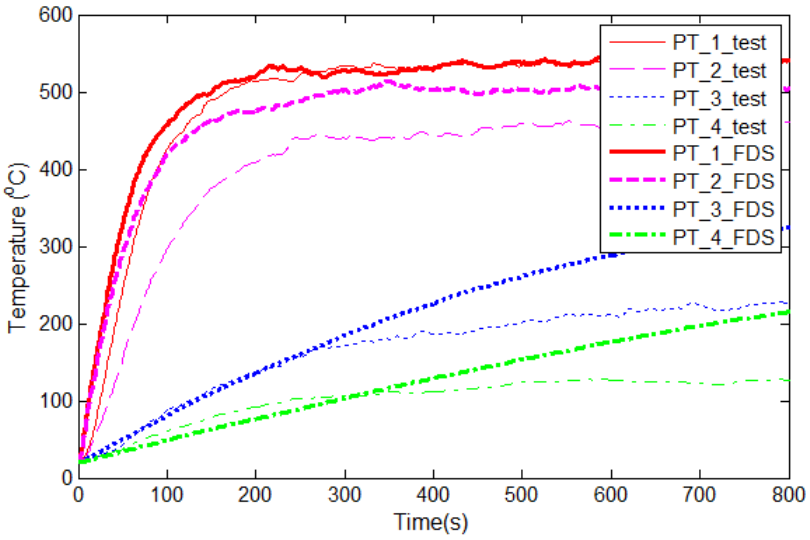

Fig. 16 Comparison between the measured and predicted plate thermometer (PT) temperatures for NFRL commissioning thermal test 3.